Beyond the Van Der Waals loop: What can be learned from simulating Lennard-Jones fluids inside the region of phase coexistence

Kurt Binder, Benjamin J. Block, Peter Virnau, and Andreas Tröster

Additional information on Am. J. Phys.

COMPUTATIONAL PHYSICS

Beyond the Van Der Waals loop: What can be learned from simulating Lennard-Jones fluids inside the region of phase coexistence

Kurt Binder, Benjamin J. Block, and Peter Virnau
Institut für Physik, Johannes Gutenberg-Universität, Staudinger Weg 7, 55099 Mainz, Germany

Andreas Tröster
Vienna University of Technology, Wiedner Hauptstr. 8-10/136, A-1040 Vienna, Austria

As a rule, mean-field theories applied to a fluid that can undergo a transition from saturated vapor at density ρ_v to a liquid at density ρ_ℓ yield a van der Waals loop. For example, isotherms of the chemical potential $\mu(T, \rho)$ as a function of the density ρ at a fixed temperature T less than the critical temperature T_c exhibit a maximum and a minimum. Metastable and unstable parts of the van der Waals loop can be eliminated by the Maxwell construction. Van der Waals loops and the corresponding double minimum potentials are mean-field artifacts. Simulations at fixed $\mu = \mu_{\text{coex}}$ for $\rho_v < \rho < \rho_\ell$ yield a loop, but for sufficiently large systems this loop does not resemble the van der Waals loop and reflects interfacial effects on phase coexistence due to finite size effects. In contrast to the van der Waals loop, all parts of the loop found in simulations are thermodynamically stable. The successive umbrella sampling algorithm is described as a convenient tool for seeing these effects. It is shown that the maximum of the loop is not the stability limit of a metastable vapor but signifies the droplet evaporation-condensation transition. The descending part of the loop contains information on Tolman-like corrections to the surface tension, rather than describing unstable states. © *2012 American Association of Physics Teachers.*
[http://dx.doi.org/10.1119/1.4754020]

I. INTRODUCTION

Statistical mechanics provides a bridge from the microscopic description of many-particle systems to their macroscopic properties.[1,2] In particular, statistical mechanics aims at computing the equation of state for a given interaction as a function of thermodynamic state variables such as the temperature T and the density $\rho = N/V$, where N is the particle number and V is the volume of the system.[3,4]

For most cases of interest no accurate methods exist to perform this task by analytical calculations.[3] The advent of computer simulation methods such as Monte Carlo and molecular dynamics provide the toolkit needed to solve problems in classical statistical mechanics.[3,5–7] However, progress has often been hampered by the misconceptions inherited from approximate theories, which have led some scientists to misinterpret results from experiments and simulations.

An archetypical example of such a misinterpretation involves the van der Waals loop, which appears in the van der Waals equation of fluids[8] and is taught in the context of the condensation of a saturated vapor. Similar loops appear in more sophisticated theories of fluids such as density functional theory and integral equation theories, and the reality of van der Waals loops is taken as a well-established fact by many researchers. Because computer simulations invariably produce loops in isotherms of intensive thermodynamic variables as a function of density,[9,10] the interpretation of such loops as van der Waals loops is almost irresistible.

However, such an interpretation is incorrect. Computer simulations yield (apart from statistical errors that can be reduced by running the simulation longer) exact results for finite size systems.[5–7] Rigorous arguments of statistical mechanics show that in the thermodynamic limit $N \to \infty$ and $V \to \infty$ with $\rho = N/V = $ constant, the thermodynamic potential is a convex function of the density ρ.[1] This property is invoked in the van der Waals context by making the *ad hoc* double tangent construction, eliminating the free energy hump in between the vapor density ρ_v and the liquid density ρ_ℓ or, equivalently, eliminating the metastable and unstable parts of the van der Waals loop by the Maxwell construction.[1,2] The exact results from computer simulations should not give the metastable or unstable parts of a chemical potential μ versus ρ isotherm. The entire loop is perfectly stable,[9–14] including the sections where $(\partial \mu / \partial \rho)_T$ is negative. The explanation for the occurrence of loops is that computer simulations are for systems for which both N and V are finite, and the loop is due to finite size effects.[12–14] Consequently, the free energy hump that inevitably results from a simulation in the canonical (N,V,T) ensemble for $\rho_v < \rho < \rho_\ell$ is a finite size effect as well.[12,13] It results from interfacial effects related to two-phase coexistence in the simulation box and hence is proportional to a surface to volume ratio. For finite N and V, we will always observe both a loop in the μ versus ρ isotherm, and a hump in

the thermodynamic potential in the two-phase coexistence region. Both these features vanish only in the thermodynamic limit, when the straight lines $\mu = \mu_{\text{coex}}$ of the Maxwell construction and the double tangent construction emerge.

This consideration is not unique to the vapor-liquid transition, and can be generalized to any first-order transition, because at such a transition we always have to traverse a two-phase region between two coexisting phases when we choose the density of an extensive thermodynamic variable as a control parameter.[1–3]

The maximum of the $\mu(\rho)$ isotherm observed in a simulation should not be interpreted as a spinodal point separating metastable from unstable states,[3] because all parts of the simulated isotherm are thermodynamically stable. How should we interpret such a maximum? As we shall see, the answer is that this maximum at some density ρ_1 is the signature of the droplet evaporation-condensation transition.[15–18] For $\rho_v < \rho_1$, the system is in a homogeneous vapor state, and for $\rho > \rho_1$ inhomogeneous two-phase configurations prevail where a droplet coexists with the surrounding supersaturated gas. In the thermodynamic limit, $\rho_1 \to \rho_v$ and the height of the maximum vanishes.

The outline of the remainder of the paper is as follows: In Sec. II, we recall the main properties of the van der Waals theory. Section III describes the isotherms and the thermodynamic potential for the truncated and shifted Lennard-Jones fluid. Section IV discusses the information on interfacial free energies that we can extract from such data, and Sec. V summarizes our results and discusses related considerations for other phase transitions. The Appendix gives some details on the non-standard parts of the simulation algorithms and their implementation.

II. SUMMARY OF VAN DER WAALS THEORY

The free energy density $f \equiv F/V$ per unit volume according to the van der Waals theory can be written as[1,2,4]

$$f_{\text{vdw}}(T,\rho) = k_B T \rho \ln\left(\frac{\lambda^3 \rho}{1 - \rho/(3\rho_c)}\right) - k_B T \rho - \frac{9}{8} k_B T_c \frac{\rho^2}{\rho_c}, \tag{1}$$

where λ is the thermal de Broglie wavelength of the fluid particles, and the molecular parameters have been eliminated in favor of the critical density ρ_c and the critical temperature T_c. The pressure $p = -(\partial F/\partial V)_{N,T}$ is thus

$$p = \frac{\rho k_B T}{1 - \rho/(3\rho_c)} - \frac{9}{8} k_B T_c \frac{\rho^2}{\rho_c}, \tag{2}$$

and the chemical potential μ becomes

$$\mu = \left(\frac{\partial F}{\partial N}\right)_{T,V} = \left(\frac{\partial f}{\partial \rho}\right)_{T,V} = k_B T \ln \frac{\lambda^3 \rho}{1 - \rho/(3\rho_c)}$$
$$+ \frac{k_B T \rho/(3\rho_c)}{1 - \rho/(3\rho_c)} - \frac{9}{4} k_B T_c \frac{\rho}{\rho_c}. \tag{3}$$

The expansion of Eqs. (1)–(3) around ρ_c, which is accurate when T is close to T_c,[19] yields

$$f_{\text{vdw}} = f_c + \mu_c(\rho - \rho_c) + \frac{9}{8} k_B T_c \rho_c \left(\frac{T}{T_c} - 1\right)\left(\frac{\rho - \rho_c}{\rho_c}\right)^2$$
$$+ \rho_c k_B T_c \frac{9}{64}\left(\frac{\rho - \rho_c}{\rho_c}\right)^4 + \cdots, \tag{4}$$

where f_c and μ_c are the free energy density and chemical potential at the critical point. For the chemical potential and the pressure, we obtain

$$\mu = \mu_c + k_B T_c \rho_c \frac{9}{4}\left(\frac{\rho - \rho_c}{\rho_c}\right)\left[\frac{T}{T_c} - 1 + \frac{1}{4}\left(\frac{\rho - \rho_c}{\rho_c}\right)^2\right], \tag{5}$$

$$\frac{p - p_c}{p_c}\left(2 - \frac{\rho - \rho_c}{\rho_c}\right) = 8\left(\frac{T}{T_c} - 1\right)\left(1 + \frac{\rho - \rho_c}{\rho_c}\right)$$
$$+ 3\left(\frac{\rho - \rho_c}{\rho_c}\right)^3, \tag{6}$$

where $p_c = 3\rho_c k_B T_c/8$).[2] From Eqs. (5) and (6), we recognize that both $\mu - \mu_c$ and $p - p_c$ contain terms in $(\rho - \rho_c)^3$ for $T = T_c$ and develop loops if we consider isotherms for $T < T_c$.

Because coexisting vapor (v) and liquid (ℓ) phases must be at the same chemical potential, we conclude that $\mu_v = \mu_\ell = \mu_c$ slightly below T_c, and hence the coexisting phases are obtained by setting the square bracket in Eq. (5) equal to zero. We solve for ρ and obtain the two solutions

$$\rho_v \approx \rho_c(1 - 2\sqrt{1 - T/T_c}) \text{ and } \rho_\ell = \rho_c(1 + 2\sqrt{1 - T/T_c}). \tag{7}$$

The critical exponent β is defined by $\rho - \rho_c \propto (1 - T/T_c)^\beta$, and thus we obtain the mean-field result $\beta = 1/2$. The extrema of the loop, which define the spinodal points found from $\partial \mu/\partial \rho)_T = 0$, occur at

$$\rho_v^s = \rho_c\left(1 - \frac{2}{\sqrt{3}}\sqrt{1 - T/T_c}\right), \tag{8a}$$

$$\rho_\ell^s = \rho_c\left(1 + \frac{2}{\sqrt{3}}\sqrt{1 - T/T_c}\right). \tag{8b}$$

The values of these extrema are $(\mu^s - \mu_c)/(k_B T_c \rho_c) = \pm\sqrt{3}(1 - T/T_c)^{3/2}$.

As an example, Fig. 1 shows the thermodynamic Landau potential per unit volume, $f_{\text{Landau}} \equiv f - \mu\rho$, and the chemical potential $\mu(\rho, T)$ plotted versus ρ at $T/T_c = 0.78$ as given by the van der Waals theory

$$f_{\text{Landau}} = f_{\text{vdw}}(\rho, T) - f_c - (\rho - \rho_c)\mu_c. \tag{9}$$

The "folklore" interpretation of the double-well in f_{vdw} and the loop in terms of metastable and unstable states is included, even though there is no sound physical basis for such an interpretation because thermodynamic functions are well defined only in thermal equilibrium. Rigorous methods of statistical mechanics yield for the region between ρ_v and ρ_ℓ in Fig. 1 only the physically correct horizontal lines for these curves.[20]

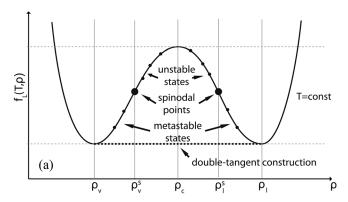## III. DOUBLE-WELL POTENTIALS AND THE LOOPS IN ISOTHERMS OBSERVED IN SIMULATIONS: WHAT DO THEY MEAN?

As an example, we consider a fluid whose particles interact pairwise with the truncated and shifted Lennard-Jones potential

$$u(r) = \begin{cases} 4\varepsilon\left[\left(\frac{\sigma}{r}\right)^{12} - \left(\frac{\sigma}{r}\right)^6 + C\right] & (r \leq r_c) \\ 0, & (r > r_c) \end{cases} \tag{10}$$
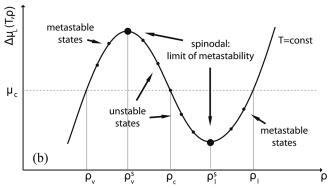
Fig. 1. Plot of the Landau potential $f_{Landau}(\rho, T)$ and the chemical potential $\mu(\rho, T)$ versus density, as given by Eqs. (5) and (6).

Here, r is the distance between the particles, ε describes the strength, and σ describes the range of the potential. For computational efficiency, the potential is cut off at $r = r_c$ but is shifted by the constant C to make it continuous at $r = r_c$. In the following a small value for r_c is chosen, namely, twice the distance of the minimum of $u(r)$, that is, $r_c = 2.2^{1/6}\sigma$. In this case $C = 127/16384$. For this choice, the critical temperature has been estimated to be $T_c = 0.999\varepsilon/k_B$.[21] Only the untruncated Lennard-Jones potential can be taken as an almost realistic description of the interaction between atoms in rare gases such as neon, argon, and krypton, or between almost spherical molecules such as methane. Although the value of T_c for the potential in Eq. (10) is about 30% lower than the corresponding value[22] for the untruncated potential, if ε and σ are chosen such that the experimentally observed critical temperature and critical density for these systems coincide with T_c and ρ_c, Eq. (10) reproduces the thermal properties of these systems very well over a wide temperature range.[23] Not only are the (Ising-like) critical exponents[24] nicely reproduced but so are the temperature dependence of the coexistence curve $\rho_v(T)$ and $\rho_\ell(T)$ in the (ρ, T) plane, the saturation pressure $p_{coex}(T)$, and the interfacial tension $\gamma_{v\ell}(T)$ between coexisting vapor and liquid.[23] Thus, Eq. (10) is both a toy model of statistical mechanics and a model that describes the properties of some simple but real systems. In the following, we will choose units such that $\sigma = 1$.

We now discuss a Monte Carlo simulation of the model in the grand canonical (μVT) ensemble and use a cubic $L \times L \times L$ box with periodic boundary conditions in all directions to avoid surface effects. The simulation samples the probability distribution $P_{\mu VT}(N)$ of observing particle number N in the system. We shall show that rich information on phase coexistence can be deduced from this basic quantity.

The basic steps of the grand canonical Monte Carlo algorithm[7] are straightforwardly implemented. Assume the system is in a state with N particles and $\vec{X} = (\vec{x}_1, \ldots, \vec{x}_N)$ represents the coordinates of the particles in the simulation box. We first generate a pseudo-random number to decide whether an insertion step, $N \to N + 1$, or a deletion step, $N \to N - 1$, should be attempted. If it is an insertion step, a random position $\vec{x}_{N+1}$ for the new particle is chosen; if it is a deletion step, the index i of the particle to be considered for deletion is randomly assigned. In this way, a trial configuration $\vec{X}'$ is generated, and the program computes the energy difference $\Delta U = U(\vec{X}') - U(\vec{X})$ between the trial configuration and the original configuration $\vec{X}$, where $U(\vec{X}) = \sum_{i<j} u(r_{ij})$. In practice, most pairs (i,j) are not affected by the change $\vec{X} \to \vec{X}'$, and thus we need to check only the immediate neighborhood of the particle, that is, inserted or deleted. At this point, the advantage of choosing a short-range truncated potential as in Eq. (10) rather than the full Lennard-Jones potential should be clear. The details of the actual implementation of this step (such as Verlet neighbor lists and cell lists) are well documented[7,25] and will not be described here. Then, the Metropolis test is made where a random number r equally distributed in the unit interval [0,1] is drawn and compared with the acceptance probability $W_{N \to N+1}$ or $W_{N \to N-1}$, respectively. These acceptance probabilities are

$$W_{N \to N+1} = \min\left\{1, \frac{V}{(N+1)\lambda^3}\exp[-(\Delta U - \mu)/k_B T]\right\},$$

(11a)

$$W_{N \to N-1} = \min\left\{1, \frac{N\lambda^3}{V}\exp[(\Delta U - \mu)/k_B T]\right\}.$$

(11b)

If r is less than the acceptance probability, the trial configuration is accepted; otherwise it is rejected, and the old configuration is counted once more for any averaging. This Monte Carlo move is repeated many times.

If we implement this standard grand canonical algorithm, for μ close to $\mu_{coex}(T)$ where the vapor and liquid phases can coexist, we find that $P_{\mu VT}(N)$ is always strongly peaked near $\langle N \rangle_{\mu VT}$ such that $\rho = \langle N \rangle_{\mu VT}/V$ is either ρ_v or ρ_ℓ. It is not straightforward to sample the full distribution $P_{\mu VN}(T)$ at all intermediate values of N corresponding to densities ρ in the two-phase coexistence region, $\rho_v < \rho < \rho_\ell$. We wish to construct a free energy function that is the analog of $V f_{Landau}(\rho, T)$ in Eq. (9) but is exact for the chosen volume given by

$$F(N, V, T) = -k_B T \ln P_{\mu VT}(N) + \mu N + F_0,$$

(12)

where F_0 is an unimportant constant. To find $F(N,V,T)$, we need to bias the sampling to force the system into the two-phase coexistence region. This biasing can be done conveniently by a method known as *successive umbrella sampling*.[26]

The idea of this method is to subdivide the density range into several windows, which are sampled consecutively or in parallel. For instance, a window may be allowed to contain 10 or 11 particles, and we count how often the state with 11 particles is visited in comparison with the state that contains 10 particles: $P_{\mu VT}(11)/P_{\mu VT}(10)$. Grand canonical insertion or

deletion moves that result in 9 or 12 particles are rejected and the previous state is counted instead. The complete probability distribution can be obtained by multiplying these ratios

$$\frac{P(n)}{P(0)} = \frac{P(1)}{P(0)}\frac{P(2)}{P(1)}\cdots\frac{P(n)}{P(n-1)}. \tag{13}$$

In practice, we take the logarithm of both sides to avoid large numbers, which may cause problems due to limited numerical accuracy

$$\ln\left(\frac{P(n)}{P(0)}\right) = \ln\left(\frac{P(1)}{P(0)}\right) + \ln\left(\frac{P(2)}{P(1)}\right) + \cdots$$
$$+ \ln\left(\frac{P(n)}{P(n-1)}\right). \tag{14}$$

If we multiply Eq. (14) by $1/(k_BT)$ and divide it by the volume of the simulation box, we directly obtain the free energy function.

Now, it becomes apparent why a subdivision into windows is advantageous. Instead of sampling the entire range of densities at once, for which we would need to overcome a large free energy barrier, only small differences in the free energy within a window are sampled. Window sizes may be increased, but restricting the window to one size keeps the free energy differences small within a window. To further improve the accuracy, the algorithm may be combined with weighting schemes as described in Ref. 26.

We note that to obtain $P_{\mu VT}(N)$ for μ close to $\mu_{\text{coex}}(T)$, it is not necessary to make many independent runs, and we can apply standard histogram reweighting methods[27] to estimate $P_{\mu'VT}(N)$ for a μ' close to μ as follows:

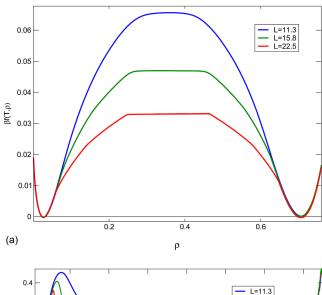$$P_{\mu'VT}(N) = \exp[(\mu' - \mu)N/k_BT]P_{\mu VT}(N). \tag{15}$$

This histogram reweighting method is very useful for finding the value $\mu_{\text{coex}}(T)$ which is unknown *a priori*. Here, we use the equal weight rule,[28,29] which states that for $\mu = \mu_{\text{coex}}(T)$ the areas beneath the peak representing the vapor (with $N \approx \rho_v V$) and the peak representing the liquid (with $N \approx \rho_\ell V$) must be equal. Although this rule was originally backed only by rough phenomenological arguments,[28] it has been rigorously justified.[29] Equation (15) is also useful for constructing the derivative of Eq. (12), by which we define the chemical potential function $\tilde{\mu}(N)$.[12]

$$\tilde{\mu}(N) \equiv \left(\frac{\partial F(N,V,T)}{\partial N}\right)_{T,V} = \mu - k_BT\left(\frac{\partial \ln P_{\mu VT}(N)}{\partial N}\right)_{T,V}. \tag{16}$$

By using these methods, we can obtain the simulation counterpart to Fig. 1, and plot $f_L(T,\rho) = [F(N,V,T) - F(V\rho_\ell, V,T)]/V$ and $\Delta\mu_L(T,\rho) = \tilde{\mu}(N) - \mu_{\text{coex}}(T)$ versus ρ as in Fig. 2. If this calculation could be done exactly in the thermodynamic limit, $F(N,V,T)$ would be the standard Helmholtz free energy, with a horizontal line between ρ_v and ρ_l.

From Fig. 2, we might be tempted to conclude that the effective potential $f_L(T,\rho)$ has a double well shape, irrespective of how large L is chosen, and similarly $\Delta\mu_L(T,\rho)$ always has a loop, overshooting $\Delta\mu_L(T,\rho) = 0$ (corresponding to $\mu = \mu_{\text{coex}}(T)$ on the vapor side, and undershooting it on the liquid side.
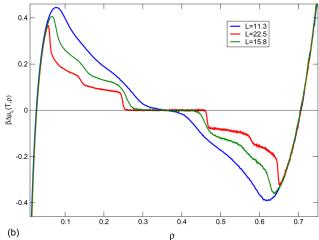

(a)

(b)

Fig. 2. Plot of the (a) free energy function $f_L(T,\rho)/k_BT$ and (b) the chemical potential difference $\Delta\mu_L(T,\rho)/k_BT$ versus the density ρ for temperature $T = 0.78T_c$, as obtained from successive umbrella sampling simulations of the truncated Lennard-Jones model, Eq. (9). The curves are for different values of L and require several days of simulation time. For reasons of clarity, only data for $L = 11.3$, 15.8, 22.5 are shown here. Data for further system sizes can be found in Refs. 13 and 14.

We note that finite size effects are negligibly small for densities $\rho < \rho_v$ and $\rho > \rho_\ell$ but are very pronounced in the two-phase coexistence region. We find that for small L the shape of $f_L(T,\rho)$ and $\Delta\mu_L(T,\rho)$ are smooth, qualitatively resembling their van der Waals counterparts, but rounded kinks are visible for larger L, which become sharper with increasing L, indicating that singularities develop as $L \to \infty$. Another remarkable feature is that for sufficiently large L, $f_L(T,\rho)$ and $\Delta\mu_L(T,\rho)$ develop strictly horizontal parts for densities near the density of the rectilinear diameter, $\rho_d = (\rho_v + \rho_\ell)/2$. The height of the plateau in Fig. 2(a) scales as $f_L(T,\rho_d) \propto 1/L$, which implies that in the thermodynamic limit the system converges to the double-tangent construction, as it should. Similarly, $\Delta\mu_L(T,\rho_d)$ is independent of L such that $\Delta\mu_L(T,\rho_d) = 0$ for all L, provided L is not too small. The range of densities ρ around ρ_d over which the plateau extends increases slowly with increasing L, and the features seen to the right and to the left of the plateau decrease in magnitude when L increases, $|\Delta\mu_L(T,\rho)| \to 0$ as $L \to \infty$ for all $\rho_v \leq \rho \leq \rho_\ell$. Thus, the simulation results converge to the results that are obtained from general and rigorous
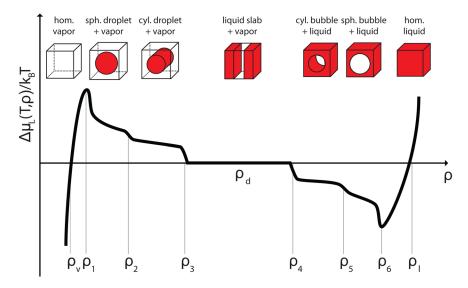
Fig. 3. Plot of the chemical potential difference $\Delta\mu_L(T,\rho)/k_BT$ versus the density ρ for $T = 0.78T_c$ and $L = 20.3$, indicating the various regimes of two-phase coexistence and the (rounded) transitions between them. Homogeneous vapor occurs for $\rho < \rho_1$. For $\rho_1 < \rho < \rho_2$ a spherical droplet coexists with the surrounding vapor in the simulation box. The transition at ρ_1 is the droplet evaporation/condensation transition. For $\rho_2 < \rho < \rho_3$ a cylindrical droplet (connected to itself by periodic boundary conditions) coexists with the surrounding vapor, and for $\rho_3 < \rho < \rho_4$ a liquid slab coexists with the vapor in such a way that two planar interfaces separating the liquid and vapor are also connected to themselves by periodic boundary conditions. For $\rho > \rho_d$ the roles of vapor and liquid are interchanged. For $\rho_4 < \rho < \rho_5$, a cylindrical vapor bubble coexists with the surrounding fluid. For $\rho_5 < \rho_6$, a spherical vapor bubble coexists with the surrounding fluid, and for $\rho > \rho_6$ there is a homogeneous fluid.
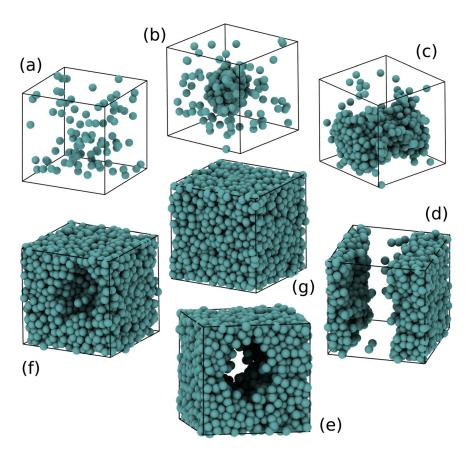

Fig. 4. Snapshots of a (a) homogeneous gas, (b) spherical droplet, and (c) a cylindrical droplet and (d) slab configuration. Also shown is a (e) cylindrical bubble, a (f) spherical bubble, and the (g) homogeneous liquid phase for $L = 15.8$ and $T = 0.78T_c$. The densities shown are $\rho = 0.02, 0.05, 0.17, 0.37, 0.58, 0.66,$ and 0.76 for (a)–(g), respectively.

arguments about phase coexistence which are valid in the thermodynamic limit,[1]

$$f_{L \to \infty}(T, \rho) = 0 \text{ and } \Delta\mu_{L \to \infty}(T, \rho) = 0 \quad (\rho_v \leq \rho \leq \rho_\ell),$$

(17)

although the convergence to this limiting behavior is slow. In any case, it is clear that computer simulations do not require any *ad hoc* recipes such as the Maxwell construction to cut-off the loop in the van der Waals isotherm in Fig. 1, whereas mean-field type theories do.

The interpretation of the structure revealed by the Landau potential $f_L(T, \rho)$ in Fig. 2(a) and the chemical potential isotherms $\Delta\mu_L(T, \rho)$ in Fig. 2(b) is clarified in Figs. 3 and 4, where in the thermodynamic limit, the strictly horizontal parts described by Eq. (17) are simply two-phase coexistence regions, described by the lever rule.[1] Thus, a state at density ρ with $\rho_v < \rho < \rho_\ell$ has a volume fraction x of liquid and a volume fraction $1 - x$ of vapor, with

$$x = (\rho - \rho_v)/(\rho_\ell - \rho_v).$$

(18)

In a macroscopic system, where surface effects due to boundaries (such as the walls of a container) are usually not considered, the shape of the coexisting macroscopic domains of vapor and liquid are disregarded. This neglect is not appropriate for a computer simulation, for which the system is finite. Although effects due to container walls are eliminated by the periodic boundaries, the effect of the interfacial free energy $\gamma_{\ell v}(T)$ between the coexisting vapor and liquid is important and controls the shape of the coexisting domains, such that at each ρ, $f_L(T, \rho)$ has a minimum.

Figure 3 shows the results, using the isotherm for $L = 20.3$ as an example. Although for $L \to \infty$ phase coexistence according to the lever rule extends over the full regime $\rho_v < \rho < \rho_\ell$, as $0 < x < 1$, this phase coexistence does not hold for finite systems. Homogeneous vapor occurs for $\rho < \rho_1$ with $\rho_1 > \rho_v$, and homogeneous liquid occurs for $\rho > \rho_6$, with $\rho_6 < \rho_\ell$. States that would be metastable in the thermodynamic limit are stable in finite systems, because the relative free energy cost of forming interfaces for $\rho_v < \rho < \rho_1$ and $\rho_6 < \rho < \rho_\ell$ is still too unfavorable. There are no metastable states in the thermodynamic limit because the system would nucleate immediately. The first appearance of a droplet at $\rho \approx \rho_1$ (or a bubble at $\rho \approx \rho_6$) occurs via a rounded discontinuous transition[18] called the droplet (bubble) evaporation/condensation transition, which we shall not discuss in detail here. Here we only mention that in the thermodynamic limit this transition converges to bulk coexistence.

In three dimensions, we expect the power laws[12,18]

$$\rho_1 - \rho_v \propto L^{-3/4} \quad \text{and} \quad \rho_\ell - \rho_6 \propto L^{-3/4}.$$

(19)

Some evidence in favor of Eq. (19) has been obtained recently by Schrader *et al.*[12] Because the slope of $\Delta\mu_L(T, \rho)/k_B T$ for T not too close to T_c at $\rho = \rho_v$ or $\rho = \rho_\ell$ is of order unity, we can conclude that $|\Delta\mu_L(T, \rho)|/k_B T$ at ρ_1 and ρ_6 has extrema whose height (or depth) also scales as $|\Delta\mu_L(T, \rho)|/k_B T \propto L^{-3/4}$. Hence, it is understandable that the structure seen in Fig. 2 vanishes slowly as L increases.

In any case, it is extremely misleading to interpret the extrema of the isotherms $\Delta\mu_L(T, \rho)$ at ρ_1 and ρ_6 as spinodal points in the sense of the van der Waals loop. We emphasize again that all parts of the loop in Figs. 2 and 3 are fully sta-

ble, and the enhancement of the stability region of vapor (for $\rho_v < \rho < \rho_1$) and liquid (for $\rho_6 < \rho < \rho_\ell$) means that in finite systems the stability of homogeneous states is enhanced in comparison with phase-separated ones. This consideration may have interesting applications in the context of nanosystems, because in such systems the effective width of a two-phase coexistence region is $\rho_1 < \rho < \rho_6$ and not $\rho_v < \rho < \rho_\ell$. We note that for such applications it is essential to consider the actual physical boundary conditions rather than periodic ones. Although many qualitative aspects of our discussion can be carried over to this setting (for example, for walls with conditions of partial wetting sphere-cap shaped droplets are found rather than full spherical ones[30,31]), an exhaustive study of this problem remains to be done.

Figure 4 presents snapshots of the two-phase states that are observed in a simulation. Due to the small size of the bubbles and droplets, these objects undergo strong statistical fluctuations in their size and in their shape. At the transition densities ρ_1, ρ_6, …, we observe fluctuations where the droplet (or bubble) completely disappears for a while and then reappears again. Similarly, at the other transition densities (ρ_2, ρ_5) there are fluctuations that carry the system from a spherical to a cylindrical shape of the interface or vice versa; near ρ_3 and ρ_4 fluctuations from cylindrical to flat interfaces and back occur. These fluctuations are rare, because free energy barriers in phase space need to be overcome, and if the simulation runs are too short, the data as shown in Fig. 2 are plagued by hysteresis effects (see Ref. 16 for an example of this problem in the context of the lattice gas model). As a result, a quantitative study of finite size rounding of all these various transitions at ρ_1, ρ_2, … remains a challenge for the future. Finite size effects on critical phenomena as well as first-order transitions between bulk phases are much better understood.[6]

For $L \to \infty$ the volume fraction x at which the droplet to cylinder or cylinder to slab-transition occurs can be found by considering the relative cost of the surface free energies as a function of density. For $L \to \infty$ the surface free energy cost of spheres of radius R is $4\pi R^2 \gamma_{v\ell}$, for cylinders of radius R it is $2\pi R L \gamma_{v\ell}$, and for slabs it is $2L^2 \gamma_{v\ell}$ (in this case, the total interfacial area is $2L^2$ because there are two planar interfaces). We have made use of the fact that for R and $L \to \infty$ the fluctuations in the shape of the domains can be neglected, as well as the curvature dependence of $\gamma_{v\ell}$.[14] As a consequence, we find that the volume fraction x_2 that corresponds to ρ_2 (the droplet to cylinder transition) becomes[11]

$$x_2 = 4\pi/81 \approx 0.155,$$

(20)

and x_3 (corresponding to ρ_3, the cylinder to slab transition) is[11]

$$x_3 = 1/\pi \approx 0318.$$

(21)

We can check from Fig. 2 that the rounded kink corresponding to the cylinder-slab transition is already close to the latter estimate, and the droplet to cylinder transition has not yet converged to a unique location. In the limit $L \to \infty$ there would just be horizontal straight lines extending from ρ_v to ρ_l.

IV. WHAT CAN WE LEARN ABOUT INTERFACIAL TENSIONS?

So far we have argued that $f_L(T, \rho)$ and $\Delta\mu_L(T, \rho)$ as shown in Fig. 2 do not contain information on metastable and unstable homogeneous states of the fluid as predicted by
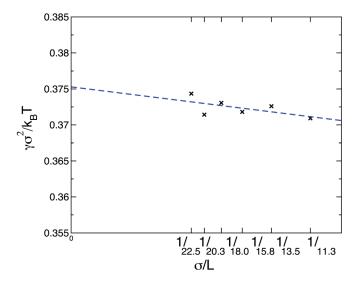
Fig. 5. The normalized surface tension $\gamma_{v\ell}\sigma^2/k_BT$ determined according to Eq. (22) from the data of Fig. 2 plotted versus σ/L. A straight line fit (as shown) yields $\gamma_{v\ell}\sigma^2/k_BT = 0.375\pm0.002$.

the van der Waals theory, but rather contain interfacial contributions corresponding to the various patterns of phase coexistence as illustrated in Figs. 3 and 4. Now, we discuss what can be learned from a quantitative study of these data about the underlying interfacial phenomena.

The simplest case is the slab configuration where the plateau of $f_L(T,\rho)$ is strictly horizontal. The latter means that a variation of ρ causes only a change in the relative amounts of the two phases, but the total interfacial area does not change. If the two interfaces can be treated as independent of each other rather than interacting, we can conclude that

$$f_L(T,\rho) = (2/L)\gamma_{v\ell}^{(L)}(T) \quad \text{and hence} \quad \gamma_{v\ell}^{(L)} = Lf_L(T,\rho)/2,$$
(22)

where $\gamma_{v\ell}^{(L)}$ is the surface tension. (Remember that $f_L(T,\rho)$ is normalized by the volume.) Figure 5 illustrates Eq. (22) for the truncated Lennard-Jones potential. We note that there must exist a systematic correction to Eq. (22), because the line that can be fitted to the data when plotted versus $1/L$ is not horizontal, but has a nonzero slope. This effect was found in the first application of this method to the two-dimensional lattice gas,[32] for which the interfacial tension is known from Onsager's exact solution.[33] Hence, this model was used as a test of this approach. The common interpretation is that the periodic boundary condition (at length scale L) cuts off the long wavelength part of the interfacial fluctuations (corresponding to capillary waves).[34] Therefore, an extrapolation of the results to $1/L \to 0$ is needed. Also note the increase of the scatter between successive estimates as L increases, which indicates the difficulty of accurately sampling the functions $f_L(T,\rho)$ and $\Delta\mu_L(T,\rho)$ near the sphere-cylinder and cylinder-slab transitions. Any systematic error due to hysteresis might lead to a slight misjudgment of the location of these transitions. An error in the location of such a transition causes a systematic over- or under-estimation of the height of the flat plateau in Fig. 2(a). In principle, this error can be reduced by a substantial increase in computational effort. However, the data of Fig. 5 show that current computer resources are still a significant limitation if we wish to obtain a relative estimate of $\gamma_{v\ell}(T)$ to better than 1%.

Although the usefulness of $f_L(T,\rho)$ to extract estimates of the interfacial tension of planar interfaces has been recognized for a long time,[32] and this technique is widely used for various systems,[35] it has been understood only recently how we can utilize the observation of phase coexistence between droplet and vapor (or bubbles and liquid) to obtain information on the interfacial tension of curved interfaces.[12–14] For a spherical droplet (or bubble), we expect a systematic variation as follows. (R is the radius of the droplet or bubble, and we consider the limit $R \to \infty$.)

$$\gamma_{v\ell}(T,R) = \gamma_{v\ell}(T,\infty)/[1 + 2\delta(T)/R + 2[\ell(T)/R]^2],$$
(23)

where $\gamma_{v\ell}(T,\infty) = v_{v\ell}^{(\infty)}(T)$, the interfacial tension of a planar interface, and the leading correction $2\delta(T)/R$ involves the Tolman length.[36] The magnitude and even the sign of this length have been controversial.[13,14,35] Because for $R \to \infty$ we can go from a droplet to a bubble via a change of sign of the radius of curvature of the interface separating the vapor and liquid, we can conclude that the sign of the leading correction to $\gamma_{v\ell}(T;R)$ for droplets must be opposite to that of bubbles. Another interesting result is that the temperature dependence of $\delta(T)$ should be weak,[37] and the length $\ell(T)$ appearing in the subleading correction scales as the bulk correlation length.[38,39] Thus, for many cases such as nucleation theory[3] for which R does not exceed the correlation length by more than a factor of 10, it is actually the term $2[\ell(T)/R]^2$ that yields the dominant curvature correction.[38,39]

The key observation that allows us to study Eq. (23) is that the presence of an equilibrium loop in $\Delta\mu_L(\rho,T)$ (see Fig. 2) for a finite system implies that for a range of chemical potentials there are three physically distinct systems at different densities at the same chemical potential (see Fig. 6). Although the density is inhomogeneous, we can explicitly verify that
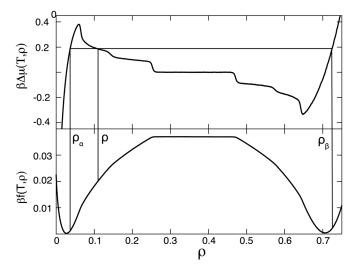

Fig. 6. Illustration of the numerical procedure for determining the density triplets ρ_α, ρ, and ρ_β for a given value of L. If we select the density ρ indicated by the vertical line near $\rho = 0.1$, then by drawing the horizontal line as shown, we can read off the homogeneous phase densities from the plot. The three solutions $(\rho_\alpha, \rho, \rho_\beta) = (0.0366, 0.1126, 0.7241)$ are highlighted by vertical lines. The state at density ρ_α is a homogeneous vapor, and the state at density ρ_β is a homogeneous liquid. The state at overall density ρ is a spherical droplet coexisting with vapor. From $f_L(T,\rho)$ shown in the lower part of the figure we can determine the free energies of the corresponding systems.

the chemical potential is homogeneous (as has been tested explicitly in Ref. 12 by applying the Widom test particle method[40]). For example, consider a system with a droplet whose overall density is $\rho = N/V$. If we consider a subbox of the system well inside the vapor region and outside the tail of the interfacial density profile of the droplet, we can conclude that the density in this subbox must be the density ρ_α (see Fig. 6) equal to the density of a uniform vapor. The vapor in the subbox is at the same chemical potential as that of the droplet, which is the same as that of the whole system. Hence, all physical properties of the vapor outside a droplet and of a homogeneous vapor must be identical. For large enough droplets, which reach a constant density in their interior, we can similarly conclude that the density in the droplet center corresponds to the liquid at density ρ_β.

Because the free energy of a system is additive with respect to contributions from its subsystems, we can write (V_α and V_β are subvolumes at phases α and β)

$$f_L(T,\rho) = \frac{V_\alpha}{V} f_L(T,\rho_\alpha) + \frac{V_\beta}{V} f_L(T,\rho_\beta) + f_L^{\text{exc}}(T,\rho),$$

(24)

where $V = V_\alpha + V_\beta$, and $f_L^{\text{exc}}(T,\rho)$ is the excess contribution related to the presence of an interface in the inhomogeneous system at density ρ (see Fig. 6). Similarly, we can use the fact that particle numbers are additive, $N_\alpha = V_\alpha \rho_\alpha$ and $N_\beta = V_\beta \rho_b$ in the inhomogeneous system to write

$$\rho(T,\Delta\mu) = \rho_\alpha(T,\Delta\mu)\frac{V_\alpha}{V} + \rho_\beta(T,\Delta\mu)\frac{V_\beta}{V} + N^{\text{exc}}/V,$$

(25)

Equation (25) indicates there can be an excess N^{exc} of particle number associated with the existence of the interface such that $N = N_\alpha + N_\beta + N^{\text{exc}}$. By definition, there is no excess volume associated with the interface, which is just a dividing surface.[34] If V_β (for a droplet, as considered in Fig. 6) is known, it is straightforward to obtain the appropriate radius R from $V_\beta = 4\pi R^3/3$.

One issue is where should we put the spherical dividing surface between the two phases α and β to find the volume V_β. If we consider the definition[34]

$$N^{\text{exc}} = 0 \quad \text{(equimolar dividing surface)},$$

(26)

a knowledge of ρ, ρ_α, and ρ_β from Fig. 6 in Eq. (25) readily yields $V_\alpha \equiv \frac{4\pi R_e^3}{3}$ and $V_\beta = V - V_\alpha$ (where the volume $V = L^3$ is known), and hence the resulting equimolar radius R_e also is known. By using these results, together with $f_L(T,\rho_\alpha)$, $f_L(T,\rho_\beta)$, and $f_L(T,\rho)$, which all can be read from Fig. 6, we can also obtain $f_L^{\text{exc}}(T,\rho)$. If we attribute the latter to the effective surface tension $\gamma_{v\ell}^{\text{eff}}(T,R_e) = f_L^{\text{exc}}(T,\rho)/(4\pi R_e^2)$, we obtain a surface tension depending on R_e, if the equimolar dividing surface is chosen to define it. This simple choice has been used in Refs. 12 and 13.

Physically, however, the most meaningful choice of a Gibbs dividing surface is not the equimolar surface defined by $N^{\text{exc}} = 0$, but the surface of tension,[34] which is defined as the dividing surface for which the corresponding interface has the minimum possible surface tension.
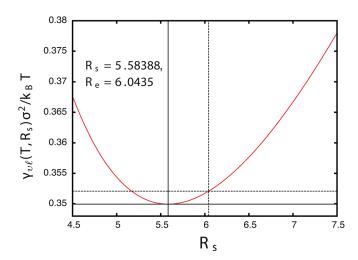

Fig. 7. Plot of $\gamma_{v\ell}(T,R)$ versus R for the state $T = 0.78T_c$, $\rho = 0.1126$ shown in Fig. 6 using Eqs. (24)–(27) with $L = 20.3$. The equimolar radius $R_e = 6.0435$ is shown as a vertical dotted line. The location of the radius $R_s = 5.5839$ of the surface of tension is shown by a full vertical line. From Ref. 14.

For a general partitioning $V = V_\alpha + V_\beta$ with dividing surface $4\pi R^2$ the interface tension $\gamma_{v\ell}(T,R)$ resulting from Eq. (24) is

$$\gamma_{v\ell}(T,R) = [V f_L^{\text{exc}}(T;R) - \Delta\mu(T,\rho)N^{\text{exc}}]/4\pi R^2.$$

(27)

As an example, Fig. 7 shows the variation of $\gamma_{v\ell}(T,R)$ with R for the parameters used in Fig. 6. We see that $\gamma_{v\ell}(T,R)$ has a minimum at $R_s \approx 5.5839$ slightly smaller than $R_e \approx 6.0431$. It is the value of the surface tension at the surface of tension that should be used when considering nucleation phenomena.[41]

We can define an effective (radius-dependent) Tolman length as[34]

$$\delta(R_s,T) = R_e(T) - R_s(T).$$

(28)

However, as a caveat we mention that in the present example $\delta(R_s,T)$ is still positive ($\delta \approx 0.45$ for $R_s \approx 5.58$), while there is evidence that for $R_s \to \infty$ the limiting value $\delta \equiv \lim_{R_s \to \infty} \delta(R_s,T)$ is negative, $\delta \approx -0.1$.[14] In other words, the effective Tolman length initially has positive values and systematically decreases. It changes sign for a very large value of R_s which is difficult to access even by simulations on a supercomputer.

Figure 8 summarizes what can be said currently on the curvature dependent vapor-liquid interfacial tension $\gamma_{v\ell}(T,R_s)$ of both droplets and bubbles. The data are normalized by the interface tension of a planar interface. If the widely used capillarity approximation of nucleation theory,[3,41] which completely neglects the curvature-dependence of the surface tension, were valid, all the data should collapse onto a horizontal straight line (at unity). The data clearly show that the capillarity approximation is inaccurate. Errors are in the range from about 5 to 25% for droplets or bubbles with radii of a few σ. (At our choice of ρ_ℓ a radius $R_s = 5\sigma$ corresponds to a droplet with about $N_\beta = 372$, and the error is about 7%.) Because $\gamma_{v\ell}^3(T,R_s)$ enters into the argument of an exponential proportional to the nucleation barrier, accurate estimates of $\gamma_{v\ell}(T,R_s)$ are necessary for a quantitatively reliable discussion of nucleation barriers.
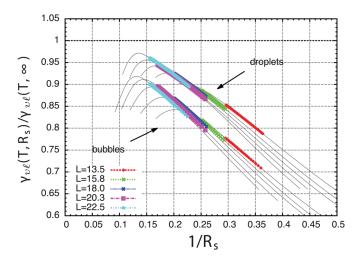
Fig. 8. Results for the reduced spherical interface tension $\gamma_{v\ell}(T, R_s)(T)$ versus $1/R_s$ at $T = 0.78T_c$, and five values of the linear dimension L. The lower data set refers to bubbles, the upper data set to droplets. The thin lines illustrate the results that we would obtain if the analysis based on Fig. 6 is carried beyond its presumed range of validity. From Ref. 14.

Figure 8 also shows that the deviations for bubbles are larger than for droplets. Some residual dependence of the data on the value of L is also evident. From Fig. 2, it is clear that some residual finite size effects are inevitable for densities close to where the droplet evaporation-condensation transition or the transition of the droplet from spherical to cylindrical shape occur. For small L, these effects become more prominent. The size dependence in Fig. 8 is not quite regular, but in view of the size effects seen in Fig. 5 for the surface tension of flat interfaces, this irregularity probably is spurious and is due to insufficient statistics. Some systematic size effects may still be hidden in the data because we use averages for estimating $\Delta\mu$ and disregard the strong (and for small systems non-Gaussian) fluctuations of this variable completely in our analysis. Nevertheless, the basic features of loops in isotherms beyond van der Waals are understood, and simulations provide tools for rich insights into interfacial phenomena.

V. CONCLUDING REMARKS

We have discussed the meaning of loops in isotherms of the chemical potential as a function of density for vapor to liquid transitions with the help of grand canonical Monte Carlo simulations and the successive umbrella sampling algorithm. In principle, the same questions could be asked using canonical Monte Carlo or molecular dynamics simulations, and sampling the chemical potential by the Widom particle insertion method. However, because conservation of the density causes very slow relaxation of long wavelength density fluctuations, the present approach is computationally more efficient.

We have described various pieces of evidence which show that the similarity of these μ versus ρ loops with the loops predicted by the van der Waals equation and related mean-field theories is only superficial. Although the loop in the latter case describes metastable and unstable homogeneous states for densities inside of the coexistence curve, the actual loop seen in simulations reflects finite size effects, and all parts of it are thermodynamically stable. For large enough

simulation volumes, we can observe various distinct regimes of various types of two-phase equilibria, with well characterized transitions between them (such as the droplet evaporation/condensation transition, transitions between spherical and cylindrical droplets (or bubbles), and transitions from cylindrical droplets (or bubbles) to slab-like states.) The usefulness of this interpretation for deducing information on the surface tension of flat and curved interfaces was demonstrated, and open problems relating to accuracy were briefly mentioned.

Studying a first-order phase phase transition using the density of an extensive thermodynamic variable as a control parameter is not restricted to the vapor-liquid transition or the closely related problem of demixing in binary fluids or solids. A classic related problem is the order-disorder transition, using, for example, the internal energy density as a control variable rather than the particle number density. In this case, we would observe loops of the inverse temperature as a function of energy density. A complication is the degeneracy of the ordered phase. For example, there is one disordered phase in the q-state Potts model, but the ordered phase is q-fold degenerate. If we apply an equal area rule to the distribution of the energy density, there are corrections of order $\ln q/V$ to the inverse temperature where the transition occurs in the thermodynamic limit, and the plateau corresponding to slab configurations is not flat.[42] To estimate interfacial free energies, it is better to focus on the inverse temperature where the plateau due to the two interfaces becomes strictly horizontal. However, obtaining information on the free energy of curved interfaces is still an open problem.

Even more difficult is the extension of these considerations to liquid-solid transitions, for which the description of the order and its degeneracy is much more complex than for the Potts model, and sampling the free energy hump throughout the two-phase-coexistence region is much more difficult. Although loops of inverse temperature versus energy are frequently observed in simulations of various systems, extracting useful information from these loops in most cases is difficult.

We have argued against considering the location of the extrema of the loops in the isotherm as valid estimates for the stability limits of metastable phases because these extrema are due to a finite size effect of the droplet/bubble evaporation/condensation transition. Metastable states that are long-lived over some parameter range are very common in nature. What is a valid estimate for the limit of metastability? Our answer is that metastability is a valid concept only in a kinetic context,[3] and we need to consider the decay of a metastable state in time via nucleation events. Because the lifetime of metastable states becomes too short to observe if the nucleation barrier is of order $\Delta F/k_B T \approx 10$ or less, our results for the surface tensions of droplets and bubbles in Fig. 8 can be used to provide estimates of nucleation barriers,[12–14] at least for vapor-liquid systems.

A double well free energy function, as described in Sec. II, is the starting point of all the renormalization group treatments of critical phenomena.[43] Do our results imply a critique of such concepts? The answer is no. The idea is that near a critical point long-range spatial correlations of the order parameter density develop. For a fluid, we can partition the system into cells of linear dimension ℓ such that ℓ is much larger than σ, but smaller than the correlation length ξ. Hence, there is no possibility for phase separation inside a cell, and a coarse-grained free energy density describing

cells of linear dimension ℓ with a homogeneous density ρ inside the cell throughout the regime $\rho_v \leq \rho \leq \rho_\ell$ makes sense. Our study pertains to the opposite limit, $L \gg \xi$. A range $\sigma \ll \ell < \xi$ exists only in the immediate vicinity of critical points.[44]

VI. SUGGESTED PROBLEM

For readers who have had some experience with Monte Carlo simulations of off-lattice models of fluids, we give a suggestion for homework.

Use the Metropolis algorithm to do a canonical Monte Carlo simulation of the truncated Lennard-Jones potential in Eq. (10). Consider a system with $L = 15.8\sigma$ and periodic boundary conditions. Choose $T = 0.78\epsilon/k_B$ and simulate a system with $N = 230$ particles using local particle displacements. Let the system evolve for some time and visualize the resulting configuration. What is the final configuration if you use 1500 particles instead? The two densities are chosen so that a liquid droplet is obtained for the first one and a slab configuration is obtained for the higher density system as indicated in Figs. 3 and 4. The goal of this exercise is to learn about the finite-size transition, which can be used to determine the surface tension and free energies of droplets.

ACKNOWLEDGMENTS

APPENDIX: THE METROPOLIS AND SUCCESSIVE UMBRELLA SAMPLING ALGORITHMS

The Metropolis algorithm
Generate a starting configuration.
Repeat:

1. Canonical Monte Carlo: displace particle at random.
2. Grand canonical Monte Carlo: attempt the insertion or deletion of a particle with equal probability.
3. Compute the energy difference between the trial and old configuration $\Delta E = E_{\text{trial}} - E_{\text{old}}$.
4. Compute the transition probability: canonical Monte Carlo: $W = \exp(-\beta \Delta E)$, where $\beta = 1/(k_B T)$
5. grand canonical Monte Carlo: W given by Eq. (11).
6. Generate a random number r in [0,1].
7. If $r < W$, accept the trial change; else reject it.
8. Increase the histogram for the observable $O(\vec{X})$.

Successive umbrella sampling
Set up a configuration in first density window. For each density window $[N, N+1]$:
Repeat:

1. Grand canonical insertion or deletion attempt. $N \rightarrow N'$.
2. If N' is outside the window, reject the trial move and take $H(N) = H(N) + 1$; else accept or reject the move according to the Metropolis criterion. If the trial move is accepted, $H(N') = H(N') + 1$; otherwise, $H(N) = H(N) + 1$.
3. Use the ratio of histograms $H(N+1)/H(N)$ to compute $P(N+1)/P(N)$.

[1]L. D. Landau and E. M. Lifshitz, *Statistical Physics, Part 1*, 3rd ed. (Pergamon Press, Oxford, 1980).
[2]D. Chowdhury and D. Stauffer, *Principles of Equilibrium Statistical Mechanics* (Wiley-VCH, Weinheim, 2000).
[3]K. Binder, "Theory of first-order phase-transitions," Rep. Prog. Phys. **50**, 783–859 (1987).
[4]P. M. Chaikin and T. C. Lubensky, *Principles of Condensed Matter Physics* (Cambridge U.P., Cambridge, 1995).
[5]*Monte Carlo and Molecular Dynamics of Condensed Matter*, edited by K. Binder and G. Ciccotti (Societa Italiano di Fisica, Bologna, 1996).
[6]D. P. Landau and K. Binder, *A Guide to Monte Carlo Simulations in Statistical Physics*, 3rd ed. (Cambridge U.P., Cambridge, 2009).
[7]D. Frenkel and B. Smith, *Understanding Molecular Simulation: From Algorithms to Applications*, 2nd ed. (Academic Press, San Diego, 2002).
[8]J. D. van der Waals, *Thermodynamische Theorie der Capillariteit in de Onderstelling van Continue Dichtheidsverandering* (Verhandlingen der Koninglijke Akademie van Wetenschappen, Amsterdam, 1893). Also see the English translation by J. S. Rowlinson, "The thermodynamic theory of capillarity under the hypothesis of a continuous variation of density," J. Stat. Phys. **20**, 197–200 (1979).
[9]L. G. MacDowell, P. Virnau, M. Müller, and K. Binder, "The evaporation/condensation transition of liquid droplets," J. Chem. Phys. **120**, 5293–5308 (2004).
[10]A. Tröster, C. Dellago, and W. Schranz, "Free energies of the ϕ^4-model from Wang-Landau simulations," Phys. Rev. B **72**, 094103-1–10 (2005).
[11]L. G. MacDowell, V. K. Shen, and J. R. Errington, "Nucleation and cavitation of spherical, cylindrical, and slablike droplets and bubbles in small systems," J. Chem. Phys. **125**, 034705-1–15 (2006).
[12]M. Schrader, P. Virnau, and K. Binder, "Simulation of vapor-liquid coexistence in finite volumes: A method to compute the surface free energy of droplets," Phys. Rev. E **79**, 061104-1–12 (2009).
[13]B. J. Block, S. K. Das, M. Oettel, P. Virnau, and K. Binder, "Curvature dependence of surface free energy of liquid drops and bubbles: A simulation study," J. Chem. Phys. **133**, 154702-1–12 (2010).
[14]A. Tröster, M. Oettel, B. Block, P. Virnau, and K. Binder, "Numerical approaches to determine the interface tension of curved interfaces from free energy calculations," J. Chem. Phys. **136**, 064709-1–16 (2012).
[15]K. Binder and M. H. Kalos, "Critical clusters in a supersaturated vapor—Theory and Monte Carlo simulation," J. Stat. Phys. **22**, 363–396 (1980).
[16]H. Furukawa and K. Binder, "Two-phase equilibria and nucleation barriers near a critical point," Phys. Rev. A **26**, 556–566 (1982).
[17]M. Biskup, L. Chayes, and R. Kotecky, "On the formation/dissolution of equilibrium droplets," Europhys. Lett. **60**, 21–27 (2002).
[18]K. Binder, "Theory of the evaporation/condensation transition of equilibrium droplets in finite volumes," Physica A **319**, 99–114 (2003).
[19]M. Rovere, D. W. Heermann, and K. Binder, "The gas-liquid transition of the two-dimensional Lennard-Jones fluid," J. Phys.: Condens. Matter **2**, 7009–7032 (1990).
[20]J. L. Lebowitz and O. Penrose, "Rigorous treatment of van der Waals-Maxwell theory of liquid-vapor transition," J. Math. Phys. **7**, 98–113 (1966).
[21]P. Virnau, M. Müller, L. G. MacDowell, and K. Binder, "Phase behavior of n-alkanes in supercritical solution: A Monte Carlo study," J. Chem. Phys. **121**, 2169–2179 (2004).
[22]J. Potoff and A. Panagiotopoulos, "Surface tension of the three-dimensional Lennard-Jones fluid from histogram-reweighting Monte Carlo simulations," J. Chem. Phys. **112**, 6411–6415 (2000).
[23]B. M. Mognetti, P. Virnau, L. Yelash, W. Paul, K. Binder, M. Müller, and L. G. MacDowell, "Coarse-grained models for fluids and their mixtures: Comparison of Monte Carlo studies of their phase behavior with perturbation theory and experiment," J. Chem. Phys. **130**, 044101-1–17 (2009).
[24]H. E. Stanley, *An Introduction to Phase Transitions and Critical Phenomena* (Oxford U.P., Oxford, 1971).
[25]M. P. Allen and D. J. Tildesley, *Computer Simulation of Liquids* (Clarendon Press, Oxford, 1989).
[26]P. Virnau and M. Müller, "Calculation of free energy through successive umbrella sampling," J. Chem. Phys. **120**, 10925–10930 (2004).
[27]A. M. Ferrenberg and R. H. Swendsen, "New Monte-Carlo technique for studying phase-transitions," Phys. Rev. Lett. **61**, 2635–2639 (1988).

[28]K. Binder and D. P. Landau, "Finite-size scaling at first-order phase-transitions," Phys. Rev. B **30**, 1477–1485 (1984).

[29]C. Borgs and R. Kotecky, "A rigorous theory of finite-size scaling at 1st-order phase-transitions," J. Stat. Phys. **61**, 79–119 (1990).

[30]D. Winter, P. Virnau, and K. Binder, "Monte Carlo test of the classical theory for heterogeneous nucleation barriers," Phys. Rev. Lett. **103**, 225703-1–4 (2009).

[31]D. Winter, P. Virnau, and K. Binder, "Heterogeneous nucleation at a wall near a wetting transition: A Monte Carlo test of the classical theory," J. Phys.: Condens. Matter **21**, 464118-1–15 (2009).

[32]K. Binder, "Monte Carlo calculation of the surface-tension for two-dimensional and 3-dimensional lattice-gas models," Phys. Rev. A **25**, 1699–1709 (1982).

[33]L. Onsager, "A two-dimensional model with an order-disorder transition," Phys. Rev. **65**, 117–149 (1944).

[34]J. S. Rowlinson and B. Widom, *Molecular Theory of Capillarity* (Clarendon Press, Oxford, 1982).

[35]K. Binder, B. J. Block, S. K. Das, P. Virnau, and D. Winter, "Monte Carlo methods for estimating interfacial free energies and line tensions," J. Stat. Phys. **144**, 690–729 (2011).

[36]R. C. Tolman, "The effect of droplet size on surface tension," J. Chem. Phys. **17**, 333–337 (1949).

[37]M. P. Anisimov, "Divergence of Tolman's length for a droplet near the critical point," Phys. Rev. Lett. **98**, 035702-1–4 (2007).

[38]S. K. Das and K. Binder, "Universal critical behavior of curvature-dependent interfacial tension," Phys. Rev. Lett. **107**, 235702-1–4 (2011).

[39]S. K. Das and K. Binder, "Thermodynamic properties of a symmetrical binary mixture in the coexistence region," Phys. Rev. E **84**, 061607-1–10 (2011).

[40]B. Widom, "Some topics in theory of fluids," J. Chem. Phys. **39**, 2808 (1963).

[41]D. Kashchiev, *Nucleation: Basic Theory with Applications* (Butterworth Heinemann, Oxford, UK, 2000).

[42]A. Tröster and K. Binder, "Microcanonical determination of the interface tension of flat and curved interfaces from Monte Carlo simulations," J. Phys.: Condens. Matter **24**, 284107-1–12 (2012).

[43]J. M. Yeomans, *Statistical Mechanics of Phase Transitions* (Clarendon Press, Oxford, 1992).

[44]A. Tröster, "Coarse grained free energies with gradient corrections from Monte Carlo simulations in Fourier space," Phys. Rev. B **76**, 012402-1–4 (2007).

Airplane Forces Apparatus

This apparatus was first described in 1932 by Prof. Ralph Hutchisson of the University of Pittsburg in the journal that later became *Journal of Applied Physics* in 1937, the year that he became its editor. The angle of attack of the airfoil can be adjusted, and the smooth flow of air is provided by a fan and a streamlining grid (not shown). Movable counterweights are adjusted to measure the amount of lift and drag produced by the wing section. The device is in the apparatus collection of Wesleyan University, and is listed in the 1950 Central Scientific catalogue at $58.00 (Notes and photograph by Thomas B. Greenslade, Jr., Kenyon College)